ECCOMAS Thematic Conference on Multibody Dynamics
July 24 - 28, 2023, Lisbon, Portugal

Physical Validation of Simulation Tools for Slender Elastic Structures

Benjamin Bauer[1], **Armin A. E. Bosten**[1,2], **Michael Roller**[1], **Joachim Linn**[1]

[1] Mathematics for Vehicle Engineering
Fraunhofer Institute for Industrial Mathematics
Fraunhofer Platz 1, 67663 Kaiserslautern, Germany
(benjamin.bauer, armin.bosten, michael.roller, joachim.linn)@itwm.fraunhofer.de

[2] Department of Aerospace and Mechanical Engineering
University of Liège
Allée de la Découverte 10, 4000 Liège, Belgium
a.bosten@uliege.be

ABSTRACT

This contribution validates different physics based software tools for the simulation of large spatial deformations of slender flexible structures. The considered simulation tools utilize discretized geometrically exact rod and shell models, with a considerable range of model properties tuned to a wider spectrum of engineering applications. We employ three benchmark tests on four simulation tools and compare the results with semi-analytic solutions from literature: The bending of a cantilever under gravity, the out of plane buckling of a predeformed beam due to coupling of bending and twist, and the lateral buckling bifurcation of a shell which is clamped such that the membrane width dimension corresponds to the direction of gravity. We examine both the reliability of the software and its behavior in these test examples. We indicate parameter ranges relevant for simulation of flexible round and flat cables, and we show that the numerical models perform well in these ranges even for coarse diszretisations.

Keywords: Slender elastic structures, rod models, cable simulation, code validation, computing methodologies.

1 INTRODUCTION

The increasing level of digitalization of industrial processes in design, functional performance layout and virtual product realization requires reliable software tools. The development of digital twins requires physically sound models, as well as efficient numerical methods to compute the behavior of elastic structures. The developers of such tools always have to compromise between physically accurate replication and fast, often real-time applicable approximations of real effects. Romero et. al [1] recently proposed a framework consisting of four benchmark tests for physical validation of simulation tools for slender elastic structures in computer graphics. These benchmarks were specifically designed such that they may be experimentally verified in a reliable manner. Adimensional scaling laws are used to robustly check the proper physical behavior of the numerical model across a large range of geometrical and material parameter combinations.

We investigate the geometrically exact rod and shell models implemented in IPS (Industrial Paths Solutions) [2], the CRod [3] and GeoXShell [4] models, and Odin [5] in three of the benchmark tests. While Odin is a flexible multibody dynamics code that computes numerical solutions *offline* with high accuracy, the other models are designed for a robust *interactive* usage of the simulation software in digital validation applications, typically employed in early phases of product development. We show that with appropriate tuning of numerical parameters, such as mesh density and number of load steps, all simulations meet the expected results based on the master curves from [1] – in particular for the geometric and material parameter ranges which are relevant to the application field. In that spirit, we study the numerical behavior of the models behind the employed software and the benchmarks and discuss the observed effects.

In section 2 we describe the beam and shell models implemented in the simulation codes of interest. Furthermore, we give meaningful ranges for material and geometry parameters. Sections 3, 4, and 5 cover the three benchmark cases: cantilever, coupling of bending and twist, and lateral buckling of shells, respectively. This includes a detailed description of the test procedure and the discussion of numerical results, which we summarize in section 6.

2 MODELS AND SOFTWARE DESCRIPTION

Beam and shell models are popular frameworks to describe slender mechanical objects. In a digital setting, their particular geometric features permit significant and necessary performance gains by reduction of the number of degrees of freedom compared to full three-dimensional continuum mechanics models. Still they capture the essential physical behavior, namely bending, torsion, and stretching deformation modes. Due to their slenderness, such structures may undergo large spatial displacements and/or rotations, while their strains remain small. Cosserat (or Simo-Reissner) and Kirchhoff-Love models allow a kinematically exact treatment of these geometric nonlinearities [6, 7, 8] and have found their way into numerous simulation tools which may be tailored to a variety of different applications, such as the simulation of hair and cloth in computer graphics, multibody system dynamics for structural mechanics, and interactive digital mock-up and VR.

The gravito-bending parameter: The main driving force of each test case is gravity. Depending on the slenderness of the beam or shell structure and the material it is composed of, the object under study will settle into a certain equilibrium shape. The situation can be summarized by one single adimensional quantity that measures the relative importance of gravitational and bending effects. It is given by

$$\Gamma_{rod} = \frac{\rho A_{\circ} g L^3}{EI} \qquad \Gamma_{shell} = \frac{\rho A_{\square} g L^3}{Dw}$$

where we denote L the length, w the shell width, A the cross-section areas, I, the second moment of area, ρ the density, E the Young's modulus, D the flexural rigidity and g the acceleration of gravity. We may interpret Γ as the ratio of the gravitational force ρALg to a bending moment $\frac{EI}{L^2}$ applied to an object. The range of meaningful values in mechanical applications is $[10^1, 10^3]$ for circular cables, bundles, and flat cables.

2.1 IPS Cable Simulation

IPS Cable Simulation is a software package that provides simulation capabilities for slender flexible mechanical components such as beams, hoses and cables. These are enhanced by several features useful for industrial applications which range from CAD to virtual assembly of cable systems. Users can interact in an intuitive fashion via grabbing the ends of a rod and moving it with the mouse or changing the configuration of attached clips. The corresponding deformed states are computed by solving a sequence of (quasi) static equilibria in real time by minimizing the elastic energy. The flexible rod is based on Kirchhoff's theory [8] and includes extensional deformation modes. The continuum formulation is discretized by a geometric finite difference scheme [2] with curve-angle kinematics closely related to the approach by Bergou et al. [9]. We will also make use of the shell model implemented in IPS. It consists in a classical geometrically exact shell discretized by finite elements [10]. Unlike its beam counterpart, the discrete equilibrium of forces and moments is solved instead of performing direct energy minimization.

2.2 CRod

The acronym CRod is a shorthand for "discrete Cosserat rod" internally used by its developers at Fraunhofer ITWM and FCC. Its discrete kinematics are constructed such that geometric properties are conserved after a finite difference discretization on a staggered grid by taking inspiration from discrete differential geometry. The CRod model was first suggested in [11] in the context of

dynamic simulation of slender viscoelastic rods. Just as before, quasi-static equilibria are found by directly minimizing the elastic energy. Some comparisons with semi analytic solutions have already been made [3].

2.3 GeoXshell

GeoXshell is a shell model introduced by Roller et al. in [4] with the efficient and robust simulation of flat cables in mind. The elastic energy from the shell continuum is discretized and applied displacements enter the formulation as simple linear constraints. Hence, in the spirit of *IPS Cable Simulation* and the CRod, quasi-static equilibria are obtained by sequentially solving a constrained minimization problem. Roller et al. also show interesting performance gains with respect to traditional finite element algorithms.

2.4 Odin

Odin is a research code for the simulation of nonsmooth flexible multibody systems, which uses geometric methods for the description of motion, for the spatial discretization of flexible components, and for the time integration. The code is able to deal with mechanical systems composed of rigid and flexible bodies interconnected by kinematic joints and interacting through frictional contact conditions. Finite motion variables are treated as elements of the Lie group $SE(3)$. A detailed description of the implemented beam model may be found in [12]. As opposed to *IPS Cable Simulation*, it is built as a FEM code aiming at a computational mechanics public. Its main specificity is the fact that the translation and rotation variables are coupled in the kinematic description, and the equilibrium equations are solved in the local frame of reference.

3 CANTILEVER BENDING

The first benchmark is valid for testing both rod and shell models, meaning structures that are thin in two or one direction, respectively. The cantilever test, first studied in detail by Bickley [13], is a standard method for obtaining elastic material parameters in soft matter physics. It is also meaningful for validation of physics-based simulators [1].

3.1 Benchmark Description

Figure 1 illustrates the basic setup of the cantilever test. We clamp the object of interest at one end and leave the other end free in a horizontal natural configuration. This means if choosing the negative y-axis as direction of gravity, the rod centerline is aligned with the x-axis and the shell mid-surface lies in the xz-plane. Under the influence of gravity, the specimen bends downwards. The amount of bending is portrayed by the total coordinate ratio $\frac{\Delta y}{\Delta x}$ measured between the end points in deformed state. This ratio depends on the gravito-bending parameter Γ.

3.2 Simulation Results

A logarithmic plot of gravito-bending against the coordinate ratio is given in Fig. 2, where the simulations align well with the semi-analytic master curve from [1]. In this section we use the measured material parameters of a representative cable bundle Ω_{bundle} from Table 1, where $\Gamma \approx 61.3$ corresponds to gravity on earth.

We observe some characteristic deviations from the master curve for both small and large values of Γ. The former consist in plateaus and arise for the IPS simulation only. They are due to very small forces that fall below the tolerance of the numerical solver. For the implemented values the solver does not even start computing a new equilibrium. In IPS this parameter is hidden from the user and cannot be modified. The research codes Odin and CRod allow a finer tuning of numerical parameters. Nevertheless, similar behavior may be induced by choosing corresponding tolerance values.

Figure 1: Exemplary illustration of the cantilever benchmark.

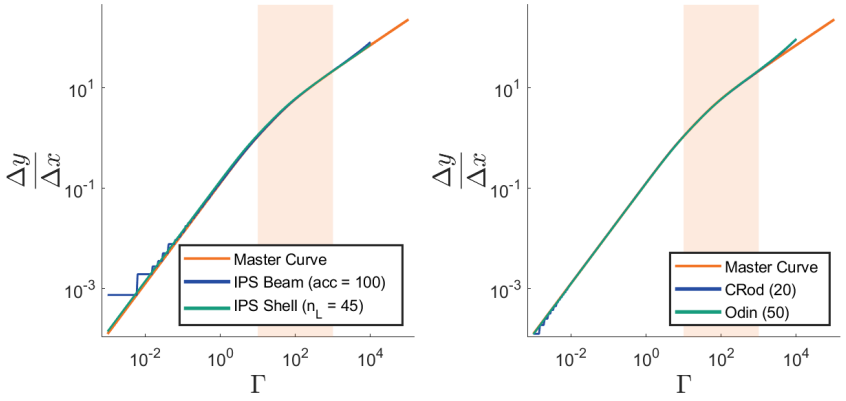

Figure 2: Simulation results of cantilever benchmark with material and geometry $\Omega_{measured}$ (rods, Table 1) and $\Omega_{combined}$ (shells, Table 2). The lines corresponding to different simulations align along the orange master curve, where the numbers in the legend indicate the number of elements in the discretization. The orange region highlights the range $\Gamma \in [10^1, 10^3]$.

Identifier	$L\ [m]$	$d\ [mm]$	$\nu\ [\,]$	$\rho\ [\frac{kg}{dm^3}]$	$EI\ [Nm^2]$	$GJ\ [Nm^2]$	$EA\ [N]$
Ω_{rod}	1.0	0.5	0.3	1273	1	0.77	1.6e7
Ω_{bundle}	1.0	6.0	0.2	2485	4.5e-2	3.75e-2	9.21e5

Table 1: Material and geometry parameters for rods in this paper. The lines correspond to the parameters proposed in [1], and a measured cable bundle. Basic and effective stiffness properties of Γ_{bundle} do not satisfy the constitutional equations of isotropic materials, as cables behave highly anisotropic (cf. [14]).

The deviations for large Γ occur since the underlying discretization is not fine enough to resolve the high curvature present in the exact solution in proximity of the clamp. Still, this issue generates different effects for the different simulation codes. Figure 3 illustrates the resulting equilibrium state for $\Gamma = 10^4$ in IPS with minimum accuracy level. In this case, the incapability to capture the correct curvature leads to elements pointing in negative x-direction such that the coordinate ratio grows away from the master curve. This behaviour strongly influences the flexible flat cable, as shown by Figure 4.

In Fig. 5 we observe a deviation from the master curve of a different nature when applying a discretization of five elements in Odin. In this case the simulated coordinate ratio falls below the master curve for large values of Γ. Here, the coarse discretization induces an artificial stiffness in proximity of the clamp, resulting in a curvature lower than in the exact solution.

The issues for large Γ both vanish when increasing the number of elements. The more elegant solution would be a local refinement procedure to avoid the loss of numerical performance.

Notably, overestimation of the coordinate ratios also arises from stretching of specimens made of a material with low tensile stiffness, for example rubber. However, these cases fall under misuse of cable simulation as a significant elongation of more than 1% would severely damage the conductor. As suggested in [1], we made sure to chose parameters such that this effect is negligible in all the computations shown in this section.

4 BEND-TWIST BIFURCATION

Numerical simulation of the bend-twist coupling of rods is a challenging task. We verify the ability of the different simulation tools to capture this effect in the present benchmark. It consists of a precurved rod possibly experiencing twist under the effect of gravity.

Identifier	$L\ [m]$	$h\ [mm]$	$E\ [MPa]$	$\nu\ [\,]$	$\rho\ [\frac{kg}{dm^3}]$
Ω_{shell}	1.0	1.0	10530	0.35	1000
Ω_{IPS}	0.1	0.2	2380	0.36	1210
$\Omega_{combined}$	0.1	0.2	10530	0.35	1000

Table 2: Material and geometry parameters for shells in this paper. The lines correspond to the parameters proposed in [1], the default values in IPS, and a combination of both.

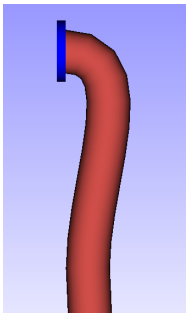

Figure 3: Characteristic misrepresentation of the curvature close to clamp for an IPS simulation at lowest accuracy.

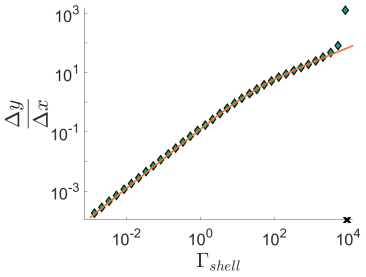

Figure 4: Cantilever simulation with an IPS shell using fifteen elements for the discretization and the material and geometry parameters Ω_{IPS}.

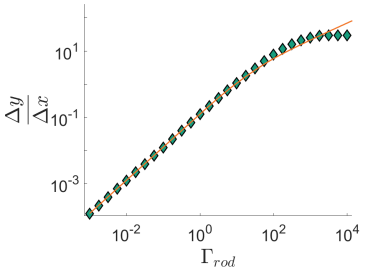

Figure 5: Cantilever simulation in Odin using five elements for the discretization and the material and geometry parameters Ω_{rod}.

4.1 Benchmark Description

In its natural stress free state the rod has a circular shape of bending radius R. It is described by the curve

$$r^\circ : \quad [0,L] \to \mathbb{R}^3, \quad s \mapsto R\left[-\sin(\tfrac{s}{R}) \quad 0 \quad -\cos(\tfrac{s}{R})\right]^T. \tag{1}$$

We allow for $L > 2\pi R$ even though self-contact inhibits a real cable to attain this configuration. Based on equation (1) the rod lies in the xz-plane initially and the tangent at $s = 0$ points in negative z-direction, which we choose to be the direction of gravity.

With gravity activated, there is a two-dimensional equilibrium occurring by plane bending of the rod. Depending on the magnitude of gravity, as well as material and geometry parameters of the rod, this configuration is stable or not. In the latter case, a small perturbation of the system (as they naturally occur in reality) leads to the rod buckling out to a three-dimensional helical shape as shown in Fig. 6.

Romero et al. [1] suggest to slightly perturb the zero-components of the curvature vector in the initial state in order to introduce disturbances. As the softwares at hand consider beam models with positions as primary variables, such a perturbation would involve numerical integration for computing the initial state. Out of simplicity, we apply a gravitational acceleration in y-direction with magnitude $\frac{|g|}{100}$ instead, before switching on the actual gravity g. After resetting the perturbation gravity in y-direction to zero, we may consider the resulting state.

For deciding whether a configuration is three-dimensional or not, we compare different measures. For each, we choose a specific density ξ, integrate it along the rod as

$$\Xi_1[\xi] = \int_0^L |\xi|\,\mathrm{d}s$$

and check if the result is greater than a prescribed threshold ε. The measures of interest are the y-coordinates of arc-length positions $\xi_y(s) := r(s) \cdot e_y$, and the Frenet torsion $\xi_\tau(s) := \tau(s)$ of the

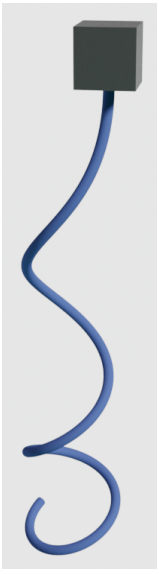

Figure 6: Exemplary illustration of the bend-twist benchmark.

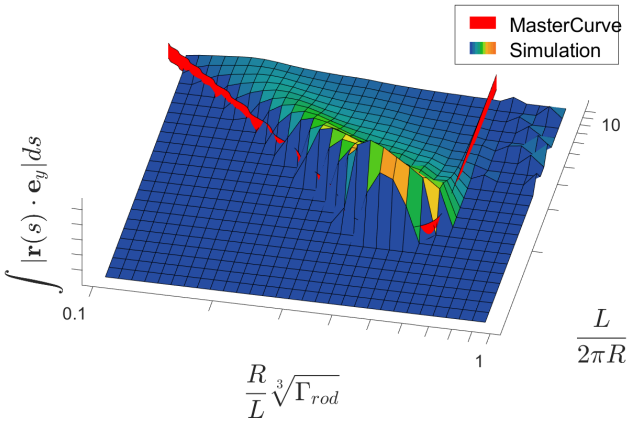

Figure 7: Integrated $y-$deviation of the equilibria in the bend-twist benchmark in Odin. Ground truth determined by the master curve displayed as red wall.

rod centre line. Latter is a classical measure to check if a curve is plane or spatial (cf. [15, sec. 1.5]). For the IPS simulations we observe that the (discretely approximated) Frenet torsion behaves equivalently to the rod twist suggested as a measure by [1].

Relevant parameters: For this benchmark we vary the parameters $\mathscr{X} = \frac{R}{L}\sqrt[3]{\Gamma}$ and $\mathscr{Y} = \frac{\varphi}{2\pi} = \frac{L}{2\pi R}$. When coiling a cable and keeping it in this spiral shape, plasticity effects lead to natural configurations close to (1) with $L > 2\pi R$. Thus the parameter range $\mathscr{Y} > 1$ is highly relevant for practical applications. Realistic Γ values for this use case lie in $[10^2, 10^3]$. The corresponding $\mathscr{X}$-values are $[4,10]/\varphi = [2,5]/\pi/\mathscr{Y}$ and depend on $\mathscr{Y}$. Thus, the interesting parameters for cable simulation lie in a corridor around $\mathscr{X}\mathscr{Y} = 1$, which is a straight line in the logarithmic phase diagram connecting $(10,1)$ and $(1,0.1)$.

4.2 Simulation Results

The results illustrated in this section have been produced by Odin, but are also representative of simulations by *IPS Cable Simulation* and the Crod model. We use the parameter set Ω_{rod} and an adaptive discretization of $100 \times y$.

Figure 7 displays $\Xi_1[\xi_y]$ for varying simulation parameters $\mathscr{X}, \mathscr{Y}$ and reveals strengths and weaknesses of this measure. While the large gradients close to the master curve for $\mathscr{Y} < 5$ capture the ground truth really well, the upper right quadrant cannot be distinguished from numerical noise by simple thresholding.

In this sense, using the criterion based on torsion gives a much cleaner height map as depicted in Fig. 8a. Still, numerical noise in the position data almost always produces finite values for $\Xi_1[\xi_\tau]$. Therefore, the threshold yielding the phase plot 8b has to be of magnitude 1 in practice. As a consequence, we believe a height map plotting $\Xi_1[\xi_\tau]$ in function of $\mathscr{X}$ and $\mathscr{Y}$ is a more illustrative and at the same time transparent representation of simulation results. Notably, a sensible combination of $\Xi_1[\xi_\tau]$ and $\Xi_1[\xi_y]$ yields the best results, using the advantages of the single criteria to balance out the weakness of the respective other.

In summary, the bend-twist benchmark is quite challenging from a numerical point of view. First, setting up the circular reference configuration for large values of $\mathscr{Y}$ requires a fine discretization

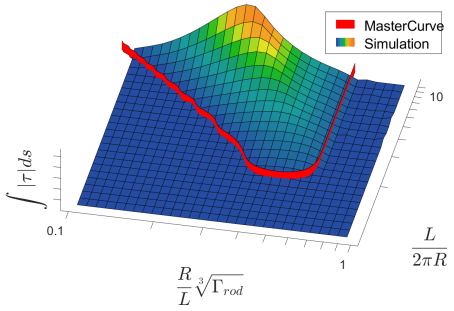

(a) Integrated torsion of the equilibria in a height map. Ground truth determined by the master curve displayed as red wall.

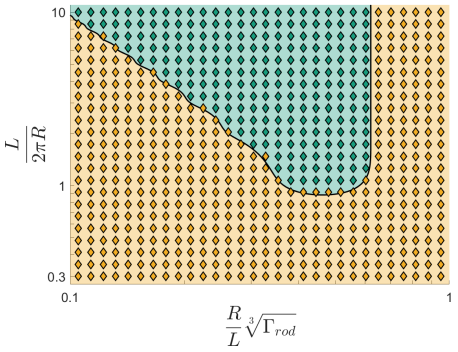

(b) Bend-Twist phase diagram with ground truth in the background and simulations as diamond shapes. Green and orange represent 3D and 2D states, respectively.

Figure 8: Overview of the bend-twist benchmark computed in Odin with $100 \times y$ elements and Ω_{rod}. Single simulations vary in the aspect ratio $\frac{L}{R}$ and the gravity-bending parameter $\frac{R}{L}\sqrt[3]{\Gamma_{rod}}$.

unless the element basis functions are tailored to such geometries. Second, disturbing the reference configuration by curvature components is not practical for every software tool. Third, the distinction between 2D and 3D depends on several factors: noise in position/torsion data, numerical issues from integration, discrete computation of the torsion and the choice of an ε-threshold.

5 LATERAL BUCKLING

A bifurcation behavior is observable for shells, as well, when employing the cantilever experiment from section 3 with the gravity directed in the width dimension of the object. In this setup, the membrane stresses prevent sagging of the free end and either lead to a planar equilibrium or a lateral buckling depending on the magnitude of present forces.

5.1 Benchmark Description

Just as in section 3, we clamp a shell such that its length and width dimensions align with x- and z-axes, respectively. This time, the gravity points in negative z-direction. As in section 4, the planar (in this case natural) state is an equilibrium between gravity and the elastic stiffness of the structure. Material and geometry data decide whether such a solution is stable or not.

We vary the gravito-bending parameter Γ_{shell} and the aspect ratio of width to length $\frac{w}{L}$ by tuning gravity and shell width, respectively. Then a lateral buckling occurs if and only if the centre of the free end has a nonzero y-coordinate.

Analogously to section 4, we require some perturbation in order to observe the bifurcation behavior. For this, we closely follow the manual of [1] and rotate the fixed boundary condition about the x-axis with a magnitude of σ. After this perturbation, we increase the gravity to its maximal value, before removing the perturbation by rotation again.

5.2 Simulation Results

First, we utilize the default material and geometry parameters in IPS Ω_{IPS} as given in Table 2. We realize both perturbation ($\sigma = 0.2$) and activation of the gravity in five steps leading to smaller changes to resolve for the numerical solver.

Figure 10 displays the simulation results for a flexible flat cable in IPS discretized by $n_L = 30$ elements in the length dimension, where the resolution of the width dimension is chosen such that each element is quadratic. In the same spirit as for the bend-twist benchmark, we illustrate the decision criterion in a height map (Fig. 9a) before thresholding with an $\varepsilon = 10^{-4}$. The red

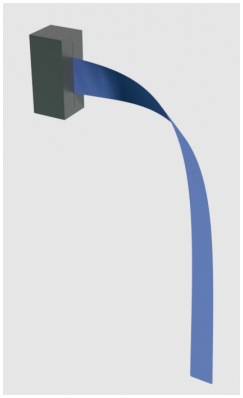

Figure 9: Exemplary illustration of the lateral buckling benchmark.

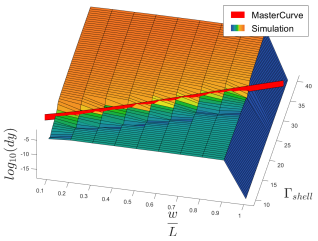

(a) Height map of the y-deviation of the end point. The ground truth is displayed as red wall indicating where the steep descent in the solution is expected.

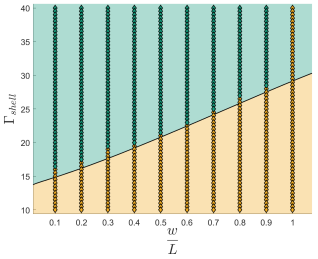

(b) Decision plot with ground truth in background and simulations as diamond shapes. Green and orange represent 3D and 2D states, respectively.

Figure 10: Overview of the lateral buckling benchmark computed for the IPS flat cable (shell) with 30 elements in length direction and Ω_{IPS}. Single simulations vary in the aspect ratio $\frac{w}{L}$ and the gravity-bending parameter Γ_{shell}.

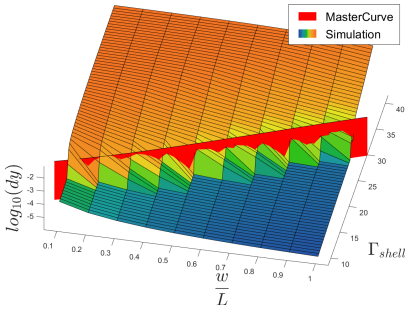

(a) Height map of the y-deviation of the end point. The ground truth is displayed as red wall indicating where the steep descent in the solution is expected.

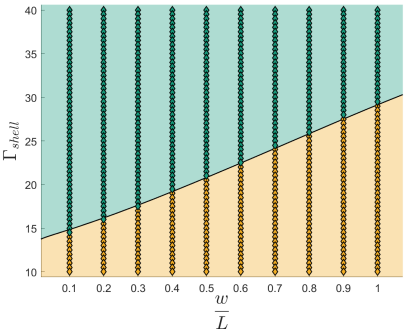

(b) Decision plot with ground truth in background and simulations as diamond shapes. Green and orange represent 3D and 2D states, respectively.

Figure 11: Overview of the lateral buckling benchmark computed for the GeoXShell with 30 elements in length direction. Single simulations vary in the aspect ratio $\frac{w}{L}$ and the gravity-bending parameter Γ_{shell}.

wall representing the master curve matches the steep descent, which corresponds to the lateral buckling, quite well for all simulations with $w < L$. In the case when we deal with a quadratic plate, the solver is not able to maintain the lateral buckling after reverting the perturbation, such that we always end up with a planar state.

We observe in Figure 11 that the GeoXShell does not struggle with $L = w$ at all, but masters the lateral buckling benchmark as depicted in Figure 11b using a mesh of medium fineness. As depicted by Figure 11a, the height map exhibits a significant descent around the master curve. Thus, locating this steep areas is a valid alternative to application of a threshold in the case of lateral buckling. Remarkably, the GeoXShell model already performs very well with a coarse discretization using eight elements in length dimension only.

5.3 Experiment Sensitivity

The lateral buckling experiment depends on a large number design parameters. Since the test case is dimensionless, we may vary the material parameters Ω just as we did for the other benchmarks. Furthermore, we can modify the mesh size, the number of load steps m_{ls}, and also verify the

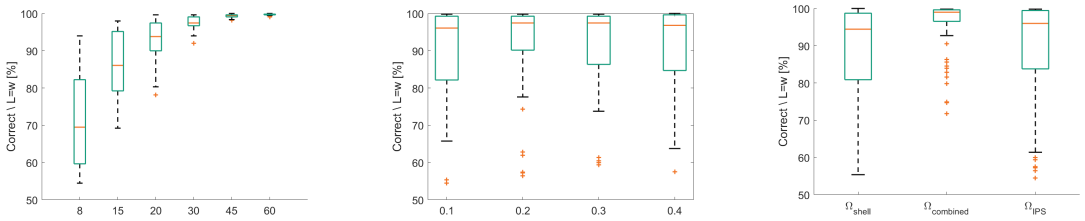

(a) Varying discretization (b) Varying perturbation angle (c) Varying material parameters

Figure 12: Boxplots illustrating the sensitivity of the lateral buckling test in IPS with respect to different design parameters. The y-axis shows the percentage of correct decisions 2D-vs-3D, neglecting $L = w$.

influence of the perturbation angle σ.

We carry out the simulation in IPS for all possible combinations of the following parameter sets

$$\Omega \in \{\Omega_{shell}, \Omega_{combined}, \Omega_{IPS}\}, \quad n_L \in \{8, 15, 20, 30, 45, 60\},$$
$$m_{ls} \in \{1, 3, 5\}, \quad \sigma \in \{0.1, 0.2, 0.3, 0.4\}$$

and compare the results. For every combination we capture the rate of correctly recognized 2D- and 3D-configurations, but exclude the cases of $L = w$.

Figure 12 displays the results in the form of boxplots grouping the simulations by one common design parameter. As expected, there is a direct relation between mesh size and solution quality. Whereas the average test with a coarse discretization $n_L = 8$ does only capture 70% of the states correctly, simulations with a discretization $n_L = 30$ succeed in at least 90% of all cases. Further convergence follows for even finder meshes. Notably, IPS is able to capture the case $L = w$ with coarse discretizations quantitatively well, whereas fine discretizations always fail.

While there is no notable difference in the solutions with different number of load steps, the suggested perturbation angle $\sigma = 0.2$ yields slightly better results than other values.

Surprisingly, the material model has the most significant impact. The material suggested in [1] combined with the default geometry in IPS performs significantly better than the other parameter sets under consideration.

6 CONCLUSION

As hoped for by the authors of [1], we followed the validation protocols therein to assess the physical realism of different simulation tools. These included the commercial software IPS and three research codes, each based on different formulations and numerical algorithms and aimed at a different audience. The main conclusions of this paper are summarized as follows:

- All codes are based on proper physical models and hence, provided a sufficiently fine discretization and appropriate tuning of numerical parameters, always yield satisfying results.
- In the range of meaningful Γ for mechanical applications, all codes perform very well with moderate and coarse discretizations.
- Even though all the material and geometric parameter combinations we used throughout the paper are equivalent from an analytic standpoint, they are not in practice. Indeed, these have an influence on performance and accuracy due to changing matrix conditioning and the need to adapt solver tolerances.

Furthermore, this paper contributes to the research literature by a detailed inspection of different benchmarks with a focus on their numerical aspects and including a discussion of relevant parameter ranges.

ACKNOWLEDGMENTS

The authors want to thank Florence Bertails-Descoubes and Sébastien Neukirch for insightful discussions and advice on the benchmarks presented in this work.

REFERENCES

[1] Romero, V., Ly, M., Rasheed, A.H., Charrondière, R., Lazarus, A., Neukirch, S., Bertails-Descoubes, F.: Physical validation of simulators in computer graphics: A new framework dedicated to slender elastic structures and frictional contact. ACM Trans. Graph. **40**(4) (2021)

[2] Linn, J., Schneider, F., Dreßler, K., Hermanns, O. In: Virtual Product Development and Digital Validation in Automotive Industry. Springer, Cham (2021) 45–52

[3] Linn, J., Hermansson, T., Andersson, F., Schneider, F.: Kinetic aspects of discrete cosserat rods based on the difference geometry of framed curves. In Valasek, M., ed.: Proceedings of the *ECCOMAS Thematic Conference on Multibody Dynamics 2017*. (2017) 163–176

[4] Roller, M., Cromvik, C., Linn, J.: Robust and fast simulation of flexible flat cables. In Kecskeméthy, A., Geu Flores, F., eds.: Multibody Dynamics 2019, Cham, Springer (2020) 207–214

[5] Cosimo, A., Brüls, O.: Odin: Gitlab repository. `https://gitlab.uliege.be/am-dept/odin` (2022) https://doi.org/10.5281/zenodo.7468114.

[6] Simo, J.: A finite strain beam formulation: The three dimensional dynamic problem. Part I. Comput. Methods Appl. Mech. Eng. **49**(1) (1985) 55–70

[7] Simo, J., Fox, D.: On a stress resultant geometrically exact shell model. part i: Formulation and optimal parametrization. Comput. Methods Appl. Mech. Eng. **72**(3) (1989) 267–304

[8] Dill, E.H.: Kirchhoff's Theory of Rods. Arch. Hist. Exact Sci. **44**(1) (1992) 1–23

[9] Bergou, M., Wardetzky, M., Robinson, S., Audoly, B., Grinspun, E.: Discrete elastic rods. ACM Trans. Graph. **27**(3) (2008) 1–12

[10] Ibrahimbegović, A.: Stress resultant geometrically nonlinear shell theory wić drilling rotations – Part I. A consistent formulation. Comput. Methods Appl. Mech. Eng. **118**(3) (1994) 265–284

[11] Lang, H., Linn, J., Arnold, M.: Multi-body dynamics simulation of geometrically exact Cosserat rods. Multibody Syst. Dyn. **25** (2011) 285–312

[12] Sonneville, V., Cardona, A., Brüls, O.: Geometrically exact beam finite element formulated on the special Euclidean group SE(3). Comput. Methods Appl. Mech. Eng. **268** (2014) 451–474

[13] Bickley, W.: The heavy elastica. Lond. Edinb. Dublin philos. mag. j. sci. **17**(113) (1934) 603–622

[14] Dörlich, V., Linn, J., Diebels, S. In: Flexible Beam-Like Structures - Experimental Investigation and Modeling of Cables. Springer, Cham (2018) 27–46

[15] do Carmo, M.P.: Differential geometry of curves and surfaces. Prentice-Hall, Englewood Cliffs, NJ (1976)